An industrial-scale cement rotary kiln CFD model to characterise altenative fuel combustion profiles.

Antonio Alcaide-Moreno[a], Miguel Ángel Castán-Lascorz[b] and Valter Tavares[c]

[a] Research Centre for Energy Resources and Consumption, Zaragoza, Spain, aalcaide@fcirce.es, CA
[b] Research Centre for Energy Resources and Consumption, Zaragoza, Spain, macastan@fcirce.es
[c] Secil-Outão, Setúbal, Portugal, valter.tavares@secil.pt

Abstract:

This work proposes a Computational Fluid Dynamics (CFD) model of a cement rotary kiln capable of reproducing some 3D effects which cannot be solved by simpler models. Specifically, flight behaviour and falling position of fuels particles are captured. Furthermore, detailed combustion chemistry (devolatilization, char combustion and moisture evaporation) is solved. The 64-meter-long kiln burns a blend of petcoke and Refuse Derived Fuel (RDF). Both were characterized and their properties introduced in the model. The clinker bed was simplified by fixing a temperature profile, a typical approach in literature. Different air excess numbers (λ) were simulated to assess the impact on flight of particles and combustion profiles. The resulting combustion profiles give a valuable input to simpler models in which a much larger and faster set of simulations can be performed, allowing kiln operators to run several different operational scenarios.

Keywords:

Cement kiln; CFD; Refuse-Derived-Fuel; Combustion.

1. Introduction

Cement production is a major source of environmental pollution due to high energy consumption and pollutant emissions [1-3]. To reduce its impact, studies have focused on using waste-derived fuels and biomass, as well as oxy-fuel and oxy-coal combustion technologies. CFD modelling has been used to investigate the co-combustion of different fuels in cement rotary kiln [1-8].

One study [1] found that annulus fuel feeding results in faster devolatilization and char combustion than central tube fuel feeding. Another study [2] aimed to reduce CO_2 emissions by optimizing the combustion process through co-combusting biomass with pulverized coal and showed that oxy-fuel combustion is promising for cement production and some studies [9-11] about oxy-coal combustion in cement rotary kilns revealed that increased combustion efficiency reduces fuel consumption [11] but may lead to a decrease in the calcination time of cement [10]. Also, the amount of NOx produced increases with increasing oxygen content in the primary air [10, 11].

Waste materials have also been used as alternative fuels in cement rotary kilns, due to the depletion of fossil fuels and an increase in their cost [4]. If thermochemical processes in clinker formation want to be modelled, a mathematical model is necessary to understand and quantify the different processes occurring inside clinker bed, particularly the homogeneous processes taking place in the freeboard of the bed of material being processed [3, 4, 6, 7]. The impact of coating layers on the clinker production process within a rotary kiln burning both coal and Refuse Derived Fuel (RDF) was investigated in one study [7], showing that a thin coating profile increases the gas phase temperature in the kiln (due to the insulation effect) reducing free lime content of the final clinker product. Study carried out in [6] showed that co-combustion of coal and RDF can lead to lower gas and clinker temperatures in the sintering zone, which can affect the clinker properties. Regarding RDF properties, [5] provided a careful characterization of its flight and combustion behaviour, useful for accurate computation of co-combustion with coal.

RETROFEED EU H2020 project main objective is to enable the use of an increasingly variable, bio-based and circular feedstock in process industries (in which a cement production industry is included) through the retrofitting of core equipment and the implementation of an advanced monitoring and control system and providing support to the plant operators by means of a Decision Support System (DSS) covering the

https://doi.org/10.52202/069564-0041

production chain. In this paper, we present the first part of the development of a cement rotary kiln model, comprising careful CFD setup and simulations of a co-firing of petroleum coke (petcoke) and RDF. Results are used to obtain characteristic combustion profiles of both fuels along the kiln, to feed a simpler 1-D model which can provide fast near real time results to the DSS.

2. Materials and methods

Figure 1 shows an overview of the modelled kiln.

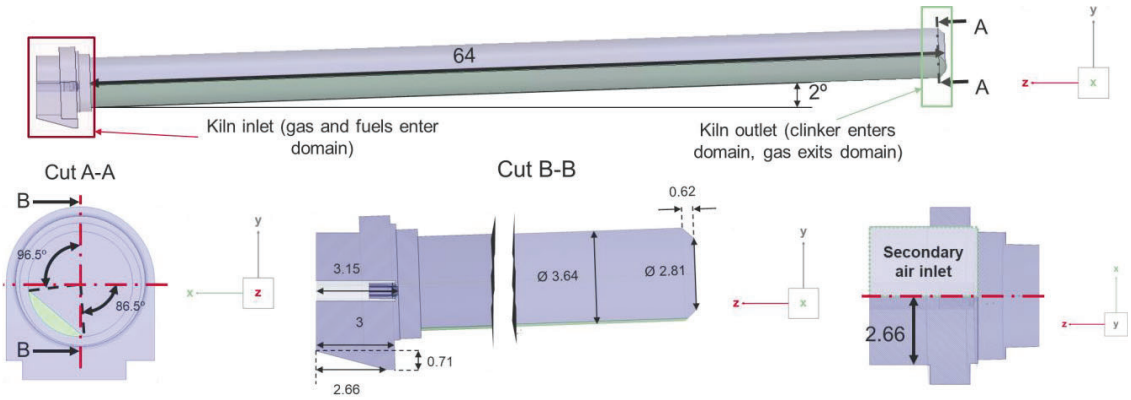

Figure 1. Modelled kiln overview and dimensions. All dimensions in meters. Kiln body is coloured in blue and actually modelled in simulations. Clinker bed is coloured in green, and it is shown only for visualization purposes, since it is not directly modelled in simulations.

2.1. Combustible characterization

In order to properly characterize the employed fuels in the modelled cement kiln, a combination of real measured and literature values was used. Petcoke and RDF are introduced by the burner.

2.1.1. Petcoke

Chemical information about petcoke is gathered in Table 1. For unmeasured values, a literature review was carried out. Properties were selected from the most similar fuel to the actually used. This was assessed by evaluating the Weighted Sum of Errors (WSE) according to Eq. (1), with all the x_i variables in unit basis (for heating values, $x_{i\,real}$ is set to one, given the importance of this term in fuel characterization). The references consulted are: [5, 7, 8, 12, 13, 14, 15, 16, 17].

$$WSE = \sum_{i=1}^{n} \left(\left| \frac{x_{i_{literature}} - x_{i_{real}}}{x_{i_{real}}} \right| \cdot x_{i_{real}} \right) \quad (1)$$

Table 1. Chemical characterisation of employed petcoke.

Parameter		Value	Unit	Source
Ultimate analysis (daf)	Carbon	85.20	%	Measured
	Hydrogen	4.04	%	Measured
	Nitrogen	1.05	%	Measured
	Oxygen	3.12	%	Measured
	Sulfur	6.59	%	Measured
Proximate analysis	Moisture	2.37	%	Measured
	Ash	0.78	%	Measured
	Volatiles	28.8	%	Normalized value of sample 9 from [13]
	Fixed carbon	68.05	%	Normalized value of sample 9 from [13]
LHV		34130	kJ/kg	Measured
Density		1423.5	Kg/m^3	Daqing petcoke from [14]
Specific heat		1000	J/(kg-K)	Average value from [18]

A granulometry analysis was also carried out, which was fitted to a Rosin-Rammler distribution. Results of granulometry are collected in Table 2, and Rosin-Rammler parameters in Table 5.

https://doi.org/10.52202/069564-0041

Table 2. Results from petcoke granulometry.

Diameter range (μm)	Mass fraction in range	Y_d: Mass fraction over diameter range
0.724 - 6.468	0.1	0.9
6.468 - 25.498	0.4	0.5
25.498 - 69.534	0.4	0.1
69.534 - 138.038	0.1	0

2.1.2.Refuse Derived Fuel (RDF)

Before introducing RDF into kiln burner, it passes through a sieve, in which particles with size over 30 mm are removed. After that, metals are also removed from the mix. From the received RDF from different suppliers all along 2020, a statistical analysis was performed to determine the typical share of components in demosite's RDF. Six samples from different suppliers were characterized, shown in Figure 2. It is noticeable the very different nature of each bucket content, confirming the heterogeneous nature of RDF fuels. As for the petcoke, data of RDF coming from demosite analysis is limited and needed to be completed with literature values. Specifically, moisture and ash content, low heating value, as well as elemental composition (ultimate analysis) is available for all the RDF received along 2019 and 2020. RDF received at demosite is divided into five main groups, gathered in Table 3. RDF/CDR is general mix of very different and heterogeneous residues. Plástico e borracha is composed of plastics and undetermined agglomerated particles, having a very high moisture content. Fluff are textiles from different sources. Materiais Impróprios p/Consumo are different residues with a similar aspect to fines as defined by [5]. They are present in demosites silos as a negligible fraction. RDF pellets are present as a low fraction in demosite silos.

From all the suppliers' lorries that arrived at demosite's facilities in 2020, the total quantity of RDF of the different groups described above is gathered in Table 3. The main difference between RDF and petcoke is about the heterogeneity of particles composing it. To properly characterize particles shape and size distribution of RDF is a very challenging task. Together with samples characterization, a literature review was done to fulfil this task. Following [5], it was found that a proper way for defining RDF particles is splitting them into five main groups of particles, namely 3D plastics, 2D foils, paper and cardboard (P&C), textiles and fines (which are unclassifiable particles smaller than ~2mm).

Table 3. RDF types received by demosite in 2020.

RDF type	Sample from Figure 2	Tons received in 2020	Mass fraction over total tons (%)
RDF/CDR	b), d) and g)	26897.4	80.7
Plástico e borracha	e)	902.2	2.7
Fluff	c) and f)	5044.9	15.1
Materiais Impróprios p/Consumo	-	27.3	0.1
RDF pellets	-	443.5	1.3

There is a need to know the quantity of each of the five groups defined by [5] in each of the RDF types from Figure 2, so a proper shape factor and size distribution can be applied to the developed model.

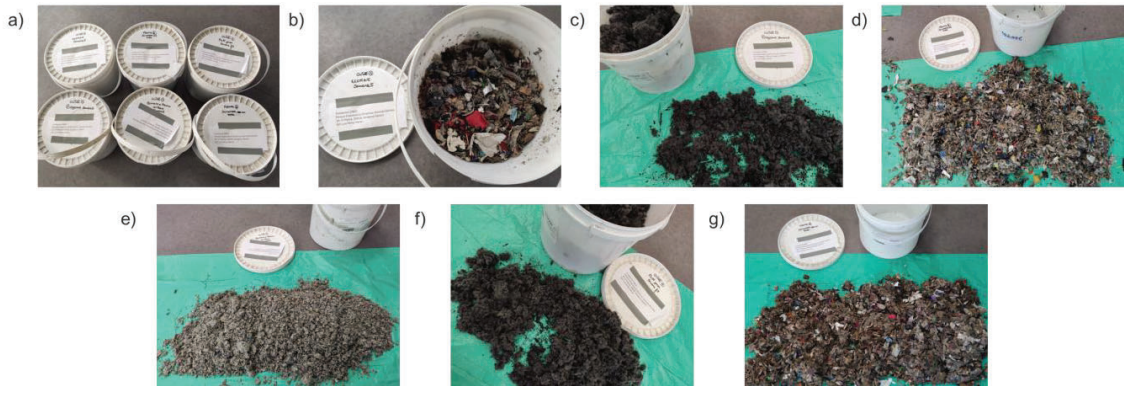

Figure 2. Samples of RDF obtained from different suppliers.

https://doi.org/10.52202/069564-0041

A sieve analysis was carried out for the three main components of RDF mix (RDF/CDR, Plástico e borracha and Fluff), which sum up a 98.6% of the total RDF used in demosite, removing previously particles with a dimension higher than 31.5 mm, which is the procedure followed in demosite. Seven sieves were used, with holes sizes of 100, 63, 45, 31.5, 16, 8 and 3.15 mm. Buckets b), e), d) and g) were sieved. Unfortunately, fluff buckets were not able to be sieved due to continuous sticking and very low density; in this case, size distribution from [5] was used. Results of the size distribution are shown in Table 4. Following the same procedure as for the petcoke, a Rosin-Rammler size distribution was obtained from the above results, obtaining the distribution parameters collected in Table 5 for each sample measured.

Table 4. Size distribution obtained from sieve analysis of RDF.

Sample from Figure 2	Type of RDF	Mass fraction (%) between sizes (mm)[1]			
		31.5-16	16-8	8-3.15	3.15-0
b)	RDF/CDR	66.7	12.4	11.8	9.1
e)	Plástico e borracha	8.4	81.4	6.7	3.5
d)	RDF/CDR	65.1	10.9	14.8	9.2
g)	RDF/CDR	77.3	8.0	8.9	4.8

[1]After removing all >31.5 mm particles and normalizing mass fractions

To properly model the chemical and combustion characteristics of RDF introduced in the developed model, it is still necessary to determine the quantity of each of the five groups given by [5]. Nevertheless, all RDF components were treated as only one, with average values of chemical parameters, due to the high computational cost of computing five different chemical species. A match between the RDF types provided to demosite and those used by [5] was done. By visual inspection, all the six samples were matched to one or various of the types of RDF reported by [5]. These matches are collected in Table 6. Percentages for RDF/CDR are the same as in RDF mixture used by [5], given the visual similarities of both mixtures.

Table 5. Rosin-Rammler distribution parameters of demosite's petcoke and RDF.

Fuel	Sample from Figure 2 (only RDF)	Diameter (μm) $\bar{d}$ (Mean)	Minimum	Maximum	n (size distribution parameter)
RDF	b)	26.0308	3.15	31.5	1.0492
	e)	12.2157	3.15	31.5	2.7679
	d)	25.9332	3.15	31.5	0.9894
	g)	28.0448	3.15	31.5	1.3136
	Fluff[1]	7.00	2.52	9.74	4.06
Petcoke	-	34.193	0.724	138.038	0.944

[1]Assumed as textiles. All data coming from [5].

Table 6. Equivalences between RDF used by demosite and the used by [5].

Demosite's RDF type	Sample from Figure 2	RDF component mass fraction (%) following [5]				
		3D plastics	2D foils	P&C	Textiles	Fines
RDF/CDR	b), d), g)	22	24	19	8	27
Plástico e borracha	e)	100[1]	0	0	0	0
Fluff	c), f)	0	0	0	100	0

[1]Despite this sample seemed to be mainly formed of fines particles, they were all agglomerated forming much larger particles that are alike 3D plastics in terms of geometry/shape.

Applying the mass fractions of Table 3 and Table 6, the resulting RDF mixture that was used in the models (only in terms of shape and physical composition; different chemical and combustion parameters are allowed to be introduced) is the shown on the right side of Figure 3. As for the petcoke, a literature review was carried out to obtain the RDF remaining properties that best fitted the ones used by demosite. It was determined that the main parameter for charaterisation of RDF combustion is moisture. Therefore, the following procedure was performed for selecting the RDF chemical properties to introduce in the models:

- A statistical analysis of all the received RDF samples in demosite during 2020 was carried out.
- To avoid abnormal values of moisture which are not representative of a typical RDF mixture, the three quartiles of the moisture content in RDF samples were obtained.

https://doi.org/10.52202/069564-0041

- Three samples of RDF were selected from the whole set: one sample with a slightly lower moisture than the first quartile one; another with a moisture almost equal to the median, and a third with a slightly higher moisture than the third quartile one.

The selected RDF samples chemical properties, as well as density, specific heat and LHV, are collected in Table 7. These will be named as RDF type 1, type 2 and type 3 in the rest of the paper.

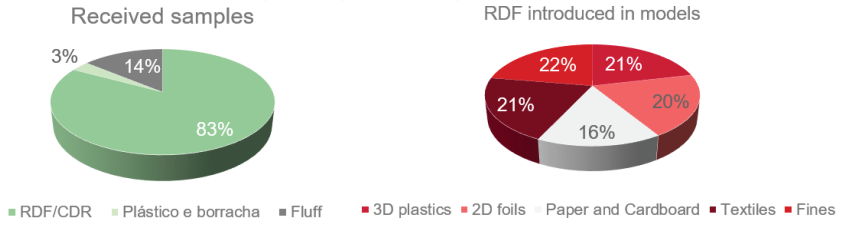

Figure 3. RDF share both in demosite's nomenclature and in reference [5] nomenclature.

Table 7. Chemical characterisation of selected RDF. Ultimate analysis basis: daf.

Parameter		Value 1	Value 2	Value 3	Unit	Source
Ultimate analysis (daf)	Carbon	75.5	49.6	57.00	%	Measured
	Hydrogen	6.67	6.17	7.23	%	Measured
	Nitrogen	1.45	1.45	1.45	%	Measured
	Oxygen	16.38	42.78	34.32	%	Measured
	Sulfur	0.00	0.00	0.00	%	Measured
	Moisture	8.58	14.82	21.06	%	Measured
Proximate analysis	Ash	6.20	210	15.20	%	Measured
	Volatiles	69.48	58.96	58.74	%	Measured
	Fixed carbon	15.74	5.22	5.00	%	Measured
LHV			28611	17345	18299	Measured
Density			852.73	852.73	852.73	Average value from [5]
Specific heat			1810	1810	1810	Average value from [5]

2.2. Simulation setup

A 3D CFD model was developed to capture the complex behaviour of fuel combustion, specifically its flight behaviour, to obtain burning profiles along its length. Three different mixes of fuels, each with two different air excess numbers (λ) were simulated. Geometry shown in Figure 1 was modelled in Ansys Fluent 2020R1. Clinker phase was not meshed nor directly simulated. Instead, it was set as a moving wall boundary condition with a fixed temperature profile. This approach has been also employed by [3]. Other researchers have used a heat flux boundary condition instead of temperature profile [6]. To avoid the prohibitive computational cost of simulating the whole burner together with the kiln cylinder, simulations of only the burner were performed, to obtain the velocity and turbulence profiles at burner outlet, to be used as boundary conditions of the whole kiln model.

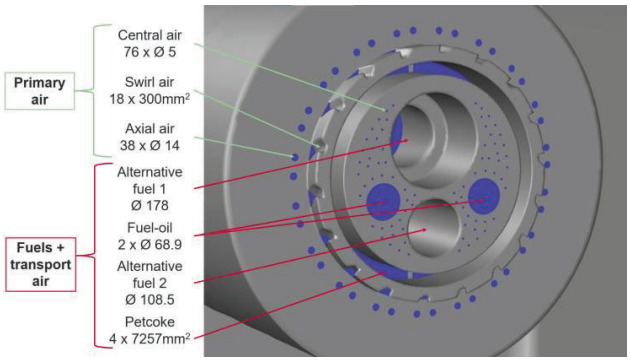

Figure 4. Modelled burner for CFD simulations.

Figure 4 shows the modelled burner. Central air holes were not meshed nor simulated, since they are so small that computational cost of a proper mesh is prohibitive. As the manufacturer of the burner ensures that 1% of flow goes through these holes, that condition was used for the whole kiln simulations. A set of

simulations of the burner alone were performed, to determine the mass flow share for each boundary. In total, five simulations were run, starting with a primary air input of 5 m/s air, and increasing in 5 by 5 steps up to 25 m/s. For all of them, the resulting mass flow share is the one collected in Table 8. Apart from that, it was also checked that, for all cases, the resulting air flow at the swirl outlet has a 0.86/1 relation in terms of tangential/axial flow direction.

Table 8. Mass flow share for each of the three primary air inlets in CFD model.

Boundary	Mass flow share (%)
Axial air inlet	63
Central air inlet	1
Swirl air inlet	36

Since primary air mass flow is fixed in the kiln to 2.83 kg/s, a simulation with the burner model was used to obtain the quantitative values of the k and ε parameters for the turbulence model in axial and swirl inlets, introduced as boundary conditions in the whole kiln model. The results are gathered in Table 9.

Table 9. Turbulence parameters for primary air inlets obtained from simulation with fixed primary air mass flow input.

Boundary	k (m^2/s^2)	ε (m^2/s^3)
Axial air inlet	132.3	896648
Swirl air inlet	243.2	1979220

Table 10 gathers some data about the resulting meshes. A detail of the whole kiln model mesh can be seen in Figure 5. Table 11 shows the type of each boundary of the kiln CFD model.

Table 10. Details of the meshes of CFD models.

Parameter	Burner model	Whole kiln model
Type of cells	Hexahedral	Hybrid polyhedral-hexahedral
Number of cells	2.99 M	2.29 M
Minimum orthogonal quality	0.10	0.27
Maximum aspect ratio	33.45	42.23

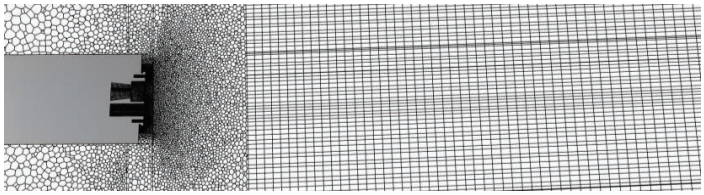

Figure 5. Example of mesh in axial cut plane of whole kiln mesh.

Table 11. Boundary types in CFD kiln model.

Boundary	Name in Figure 4 (only burner inlets)	Boundary
Axial air inlet	Axial air	Mass flow inlet
Central air inlet	Central air	Mass flow inlet
Swirl air inlet	Swirl air	Mass flow inlet
Petcoke inlet	Petcoke	Mass flow inlet
RDF inlet	Alternative fuel 1	Mass flow inlet
Secondary air inlet	-	Mass flow inlet
Outlet	-	Pressure outlet
Burner walls	-	Adiabatic wall
Clinker-gas contact interphase	-	Moving fixed-temperature wall

Details of boundary conditions are gathered in Appendix A: detailed boundary conditions in CFD simulations. Mass, momentum and energy were solved with a Reynolds Averaged Navier Stokes (RANS) approach. Turbulence was solved with the realizable κ–ε model with enhanced wall treatment [19]. Radiation is solved using the Discrete Ordinates model. Chemistry is solved with the species transport model, with one volatiles

https://doi.org/10.52202/069564-0041

species for petcoke and another for RDF. Turbulence-chemistry interaction was solved with the eddy-dissipation model [7]. Particles flight and combustion behaviour were solved with the Discrete Phase Model (DPM) ([3, 6, 7], and similar to the used in [8]). One injection for petcoke and five for RDF were used, with size distribution according to Table 5. Particles devolatilization and char combustion models parameters, as well as water droplet mass transfer model (drying of fuels) and parameters, are collected in Table 22. All values for petcoke and water are obtained from [20], whereas those for RDF come from [5].

Table 12. Combustion modelling parameters for discrete phase model in CFD simulations.

Parameter		Material		
		Petcoke particle	RDF particle	Water droplet
Vaporization temperature (K)		550	550	-
Devolatilization	Model	Single rate		-
	Preexponential factor (s^{-1})	9.59e+04	2.47e+06	-
	Activation energy (J/kgmol)	8.26e+07	1.065e+08	-
Combustion	Model	Kinetics/ diffusion limited		-
	Rate constant	5e-12	5e-12	-
	Preexponential factor (s^{-1})	0.01	0.00204	-
	Activation energy (J/kgmol)	1.05e+08	7.9423e+07	-
Thermolysis	Model	-	-	Single rate
	Preexponential factor (s^{-1})	-	-	5.13e+06
	Activation energy (J/kgmol)	-	-	8.79e+07

3. Results and discussion

One kiln operating point corresponding to typical values was simulated with values shown in Table 13.

Table 13. Common boundary conditions of inlets in CFD simulations.

Parameter	Value	Unit
Primary air flow (divided according to Table 8)	2.83	Kg/s
Petcoke transport air flow	1.17	Kg/s
RDF transport air flow	0.75	Kg/s
Petcoke particles flow	0.61	Kg/s
RDF particles flow (divided according to Figure 3)	1.94	Kg/s
Primary air temperature	49	ºC
Petcoke air and particles temperature	61	ºC
RDF air and particles temperature	34	ºC
Secondary air temperature	916	ºC

Two different excess air numbers were simulated for each RDF type, as shown in Table 14.

As a representative case, some detailed results of temperature and particle flight and reaction behaviour are shown from CFD simulation 1-1. Figure 6 shows the temperature contour of simulation 1-1. As can be seen, temperature increases due to combustion relatively far from burner, unlike traditional petcoke and low-share RDF quantities (such as those reported by [3] and [7]). This is due to the poor combustion quality of RDF, displacing the flame formation downwards. RDF's higher size and ash fraction compared to petcoke can explain this result. It can be also seen that temperature increase starts from the bottom of kiln (i.e., clinker surface), and shows a high peak of temperature in that zone. This is due to the flight of RDF particles (as will be seen in next figures): given their high size (thus, low burning rate) and non-spherical shape, they tend to

fall onto clinker surface instead of being blown away by air. This result is in agreement with the reported by [3, 6, 7]. After the first third of kiln length (~20m), flame profile widens and effectively heats homogeneously the whole domain.

Table 14. Performed CFD simulations boundary conditions.

Simulation	RDF type from Table 7	RDF power share (%)	λ
1-1	1	72.90	1.1
1-2	1	72.90	1.4
2-1	2	61.99	1.1
2-2	2	61.99	1.4
3-1	3	63.25	1.1
3-2	3	63.25	1.4

To explain the above results, Figure 7 shows the particle tracking of each type of particle introduced through the burner up to the half of kiln length. As it can be seen, only petcoke and fines (which are the smallest RDF particles) are blown by air throughout the kiln length. The rest of particles fall onto clinker bed soon, where they start to burn. Though fines are blown by air, they start burning in the same location than the rest of RDF particles. This is due to their low combustion quality (they need very high temperatures to start the reaction) in comparison with petcoke. The burning location of RDF particles explain the peak temperature found at clinker bed surface in Figure 6. These particles flight trajectories of RDF particles also found by [6].

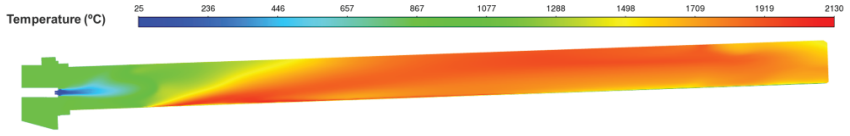

Figure 6. Temperature contours from CFD simulation in a longitudinal plane contour.

To obtain the combustion profiles from the simulations, the CFD domain was split into 64 axial slices, in which the integral of petcoke and RDF volatiles and burnout (char oxidation), as well as water evaporated from particles, was obtained. Results are shown in Figure 8.

Some general comments apply for all the simulations results:

- Petcoke devolatilization and fixed carbon burning show a well-shaped Gauss bell distribution.
- Dried water profiles show two humps. The first coincides with the higher petcoke volatiles and fixed carbon release; the second hump, higher than the first, takes place at around 10 meters, where high temperatures appear near clinker surface.
- Higher air excess show wider distributions, which reflect the higher drag force and flow speed suffered by particles, which tend to spread out their burning locations.
- Very low RDF char is burned in gas phase for all the simulated cases. This results in a burning after falling onto clinker surface, which CFD is unable to capture and has to be taken into account in some way if an accurate modelling is intended, as [3] and [6] affirm.

Something very noticeable is that, for RDF types 1 and 2, burning profiles are very similar regardless the excess air used; on the other hand, RDF type 3 shows large differences in petcoke combustion between the two air excesses simulated, but not on RDF combustion or evaporation. This may be due to the poor resolution of the discretization employed; a higher number of slices may provide less discrepancies between cases. It can be seen that the totality of petcoke combustible matter burns within gas phase in the first 10 meters of the kiln, confirming its very good burning behaviour with respect to RDF. An interesting result is that, in all the cases, RDF power is released earlier in the case with lower air excess, reflecting less drag force and speed of particles.

Another interesting result is that all RDF volatiles are released a bit later than half of the kiln (~40 m). All the RDF char that combusts in gas phase (which is very low in general) also does it mostly in the first 40 meters of the kiln. It can be also seen that, in all the cases, RDF volatiles start to be released earlier and end later in the case with λ=1.4 than in the case with λ=1.1. This may be due to the higher oxygen availability for RDF in the first part of the kiln in the case with λ=1.4, but less gas temperature is achieved (more mass of air is heated), so reaction is slower than in the case with λ=1.1. On the other hand, the opposite happens to RDF

https://doi.org/10.52202/069564-0041

char combustion. It starts later in the case with more excess air. A higher char combustion can be achieved in gas phase when increasing excess air number, particularly in the RDF type 3 case.

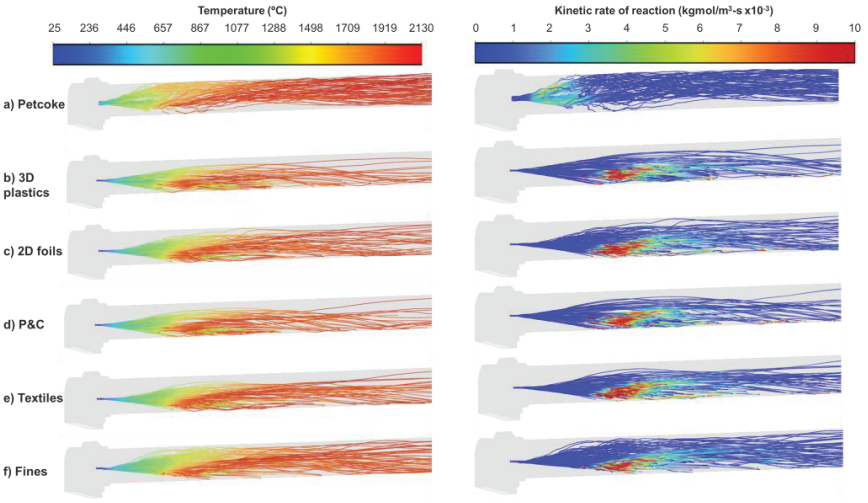

Figure 7. Trajectories coloured by temperature (left) and kinetic rate of reaction (right) of the different modelled particles within CFD, from simulation 1-1.

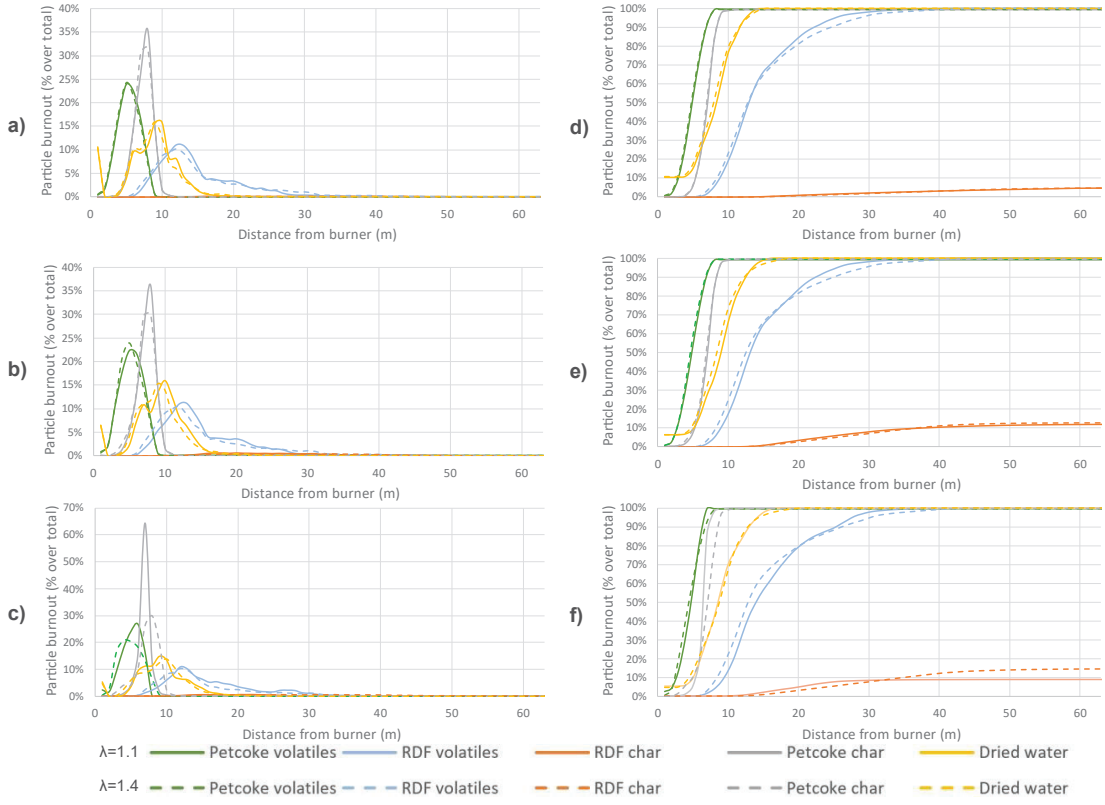

Figure 8. Burning and evaporation profiles from CFD simulations. Left: per slice profile. Right: histogram of profile. a), d) RDF type 1; b), e) RDF type 2; c), f) RDF type 3.

4. Conclusions

From the performed CFD study, some conclusions can be extracted:

- Combustion temperature increases far from the burner due to poor combustion quality of RDF, which displaces the flame formation downwards.
- Temperature increase starts from the bottom of kiln, with a high peak of temperature in that zone due to the flight of RDF particles falling onto clinker surface.
- Only petcoke and smallest RDF particles are blown by air throughout the kiln length, while the rest of particles fall onto clinker bed more or less soon, where they start to burn.
- Petcoke devolatilization and fixed carbon burning show a well-shaped Gauss bell distribution.
- Very low RDF char is burned in gas phase for all the simulated cases, resulting in burning after falling onto clinker surface.
- Burning profiles are very similar for RDF types 1 and 2 regardless of excess air used, while RDF type 3 shows large differences in petcoke combustion between two air excesses simulated.
- All petcoke combustible matter burns within gas phase in the first 10 meters of the kiln, confirming its very good burning behaviour with respect to RDF.
- All RDF volatiles are released a bit later than half of the kiln, and RDF char that combusts in gas phase also does it mostly in the first half of the kiln.
- RDF volatiles start to be released earlier and end later in the case with higher air excess.
- A higher char combustion can be achieved in gas phase when increasing excess air number, particularly in the RDF type 3 case.
- CFD seems to be a useful tool for understanding the combustion behaviour, as well as temperature profiles in the complex processes that take place inside a cement kiln which, in practice, cannot be measured in experiments due to high quantities of dust, kiln rotation and hard temperature conditions. This allows to understand and optimize their functioning.

5. Funding

This project received funding from the European Union's Horizon 2020 research and innovation programme under grant agreement No. 869939. https://retrofeed.eu/ (accessed on 11 March 2023).

References

[1] W. K. Hiromi Ariyaratne, A. Malagalage, M. C. Melaaen and L.-A. Tokheim, "CFD modelling of meat and bone meal combustion in a cement rotary kiln – Investigation of fuel particle size and fuel feeding position impacts," Chemical Engineering Science, vol. 123, no. 17, pp. 596-608, 2015.

[2] H. Mikulčić, D. Cerinski, J. Baleta and X. Wang, "Improving Pulverized Coal and Biomass Co-Combustion in a Cement Rotary Kiln by Computational Fluid Dynamics," Chemical Engineering & Technology, vol. 42, no. 12, pp. 2539-2545, 2019.

[3] B. Liedmann, S. Wirtz, V. Scherer and B. Krüger, "Numerical Study on the Influence of Operational Settings on Refuse Derived Fuel Co-firing in Cement Rotary Kilns," Energy Procedia, vol. 120, pp. 254-261, 2017.

[4] B.-J. R. M. Bisulandu and F. Marias, "Modeling of the Thermochemical Conversion of Biomass in Cement Rotary Kiln," Waste and Biomass Valorization, vol. 12, no. 2, pp. 1005-1024, 2021.

[5] B. Liedmann, W. Arnold, B. Krüger, A. Becker, S. Krusch, S. Wirtz and V. Scherer, "An approach to model the thermal conversion and flight behaviour of Refuse Derived Fuel," Fuel, vol. 200, pp. 252-271, 2017.

[6] C. Pieper, B. Liedmann, S. Wirtz, V. Scherer, N. Bodendiek and S. Schaefer, "Interaction of the combustion of refuse derived fuel with the clinker bed in rotary cement kilns: A numerical study," Fuel, no. 117048, 2020.

[7] C. Pieper, S. Wirtz, S. Schaefer and V. Scherer, "Numerical investigation of the impact of coating layers on RDF combustion and clinker properties in rotary cement kilns," Fuel, no. 283, 1 January 2021.

[8] M. Nakhaei, H. Wu, D. Grévain, L. Jensen, P. Glarborg and K. Dam-Johansen, "CPFD simulation of petcoke and SRF co–firing in a full–scale cement calciner," Fuel Processing Technology, no. 196, 2019.

[9] M. Ditaranto and J. Bakken, "Study of a full scale oxy-fuel cement rotary kiln," International Journal of Greenhouse Gas Control, vol. 83, pp. 166-175, 2019.

[10] Z. Ying, C. Lixin, L. Qiao, C. Guozan and Y. Xuchu, "Simulating the Process of Oxy-Fuel Combustion in the Sintering Zone of a Rotary Kiln to Predict Temperature, Burnout, Flame Parameters and the Yield of Nitrogen Oxides," Chemistry and Technology of Fuels and Oils, vol. 54, pp. 650-660, 2018.

[11] M. Wang, B. Liao, Y. Liu, S. Wang, S. Qing and A. Zhang, "Numerical simulation of oxy-coal combustion in a rotary cement kiln," Applied Thermal Engineering, vol. 103, pp. 491-500, 2016.

https://doi.org/10.52202/069564-0041

[12] G. Fuyan, L. Jianzhong, W. Chuancheng and Z. K. C. Junhu, “Effects of the physical and chemical properties of petroleum coke on its slurryability,” Petroleum Science, vol. 9, pp. 251-256, 2012.

[13] P. Ghetti, “DTG combustion behaviour of coal. Correlations with proximate and ultimate analysis data.,” Fuel, pp. 636-639, May 1986.

[14] Q. He, R. Wang, W. Wang, R. Xu and H. Baixing, “Effect of particle size distribution of petroleum coke on the properties of petroleum coke-oil slurry,” Fuel, no. 90, pp. 2896-2901, 2011.

[15] K. Jayaraman and I. Gokalp, “Gasification characteristics of petcoke and coal blended petcoke using thermogravimetry and mass spectrometry analysis,” Applied Thermal Engineering, vol. 80, pp. 10-19, 2015.

[16] J. Parikh, S. A. Channiwala and G. K. Ghosal, “A correlation for calculating HHV from proximate analysis of solid fuels,” Fuel, vol. 84, pp. 487-494, 2005.

[17] S. J. Yoon, Y.-C. Choi, S.-H. Lee and J.-G. Lee, “Thermogravimetric study of coal and petroleum coke for co-gasification,” Korean Journal of Chemical Engineering, vol. 24, pp. 512-517, 2007.

[18] M. Long, J. Sheng, T. Liu, D. Chen, Y. Yang, S. Gong and C. Chen, “Thermo-Physical Properties of Petroleum Coke during Calcining Graphitization Process,” in Drying, Roasting, and Calcining of Minerals, TMS (The Minerals, Metals & Materials Society), 2015, pp. 193-199.

[19] H. F. M. Elattar, Flame Simulation in Rotary Kilns Using Computational Fluid Dynamics (PhD thesis), Magdeburg: Otto Von Guericke Universität Magdeburg, 2011.

[20] M. N. Pedersen, Co-firing of Alternative Fuels in Cement Kiln Burners (PhD thesis), Technical University of Denmark, 2018.

[21] S. Chen, J. Wang and Q. Li, “Composite Design of Low Thermal Conductivity Mullite Brick for Application to Cement Kiln,” International Conference on Materials Applications and Engineering 2017 (ICMAE2017) , vol. 142, 2018.

[22] Y. A. Çengel and A. J. Ghajar, Heat and Mass Transfer. Fundamentals & Applications, New York, NY: McGraw-Hill Education, 2015.

[23] C. Lou, H.-C. Zhou, P.-F. Yu and Z.-W. Jiang, “Measurements of the flame emissivity and radiative properties of particulate medium in pulverized-coal-fired boiler furnaces by image processing of visible radiation,” Proceedings of the combustion institute, no. 31, pp. 2771-2778, 2007.

Appendix A: detailed boundary conditions in CFD simulations

Table A.1. Clinker-gas contact interphase boundary conditions.

Physics	Parameter	Value	Unit	Source
Momentum	Moving wall direction	From kiln outlet to kiln inlet	-	-
	Translational speed	0.02262	m/s	Calculation from raw meal input, kiln cross-sectional area and estimated kiln fill degree
Thermal	Condition	Fixed temperature, Eq. (A.2)	K	Curve fitting from demosite’s measurements in six different points of clinker surface
	Thermal conductivity	0.33	W/m-K	[6]
Radiation	Internal emissivity	0.8	-	[6]
DPM	Boundary condition	Trap	-	From observations

[1]x: axial direction of kiln cylinder, taking x=0 at the cylinder end near to kiln inlet

Applied fixed temperature profile is given by Eq. (A.2).

$$T(K) = 3.1822 \cdot 10^{-4}\, x^4 + 3.5854 \cdot 10^{-2}\, x^3 + 0.78137\, x^2 - 5.3164x + 1502.7 \qquad \text{(A.2)}$$

Table A.2. Kiln cylinder walls boundary conditions.

Physics	Parameter	Value	Unit	Source
Momentum	Wall motion	Stationary wall	-	-
Thermal	Condition	Convection	-	-
	Heat transfer coefficient	10	W/m2-	Typical value for natural convection

			K	
	Free Stream Temperature	27	ºC	Estimated mean temperature values along a year
	Wall thickness	0.2	m	Estimation from SECIL
	Wall density	2650	Kg/m3	[21]
Radiation	Wall specific heat	835	J/kg-K	Chrome brick, from [22] table A-8
DPM	Wall thermal conductivity	2.74	W/m-K	[21]

Table A.3. Burner and hood walls boundary conditions.

Physics	Parameter	Value	Unit	Source
Momentum	Wall motion	Stationary wall	-	-
Thermal	Condition	Heat flux	-	-
	Heat flux	0	W/m^2	Negligible participation in convection and radiation heat transfer
Radiation	Internal emissivity	0.6	-	Typical value for aluminium, from [22] table A-18
DPM	Boundary condition	Reflect	-	From observations

Table A.4. Thermophysical and radiation properties of materials employed in CFD simulations.

Material	Parameter	Value	Unit	Source
Gas mixture	Specific heat	Mixing law	-	[5]
	Thermal conductivity	Mass weighted mixing law	-	-
	Viscosity	Mass weighted mixing law	-	[5]
	Absorption coefficient	WSGGM method	-	[7], [5]
	Scattering coefficient	0.54	-	Derived from [23]
Petcoke particle	Emissivity	0.7	-	[23]
	Scattering coefficient	0.54	-	[23]
RDF particle	Emissivity	0.877	-	[5]
	Scattering coefficient	0.54	-	[23]

https://doi.org/10.52202/069564-0041